Combining in-cylinder pressure and 1D simulation tools to understand the combustion characteristics of natural gas in pre-chamber ignition systems for energy generation

Antonio García[1,*], Joaquín De la Morena[1], Javier Monsalve-Serrano[1], Rafael Lago Sari[1], Per Tunestal[2]

Energy Conversion and Management

Volume 240, 15 July 2021, 114262

https://doi.org/10.1016/j.enconman.2021.114262

[1]CMT-Motores Térmicos, Universitat Politècnica de València. Camino de Vera s/n, E-46022, Valencia, Spain.

[2]LKCFP Engine Research Center, Lund University. Ole Römers Väg 1 (vån 5) Sweden.

Corresponding author (*):
Dr. Antonio García (angarma8@mot.upv.es)
Phone: +34 963876574
Fax: +34 963876574

Keywords

Pre-chamber, natural gas combustion, heat release, 1-D simulation

Abstract

Recent outlooks suggest a long-term relevance of internal combustion engines for both power generation and transportation. Nonetheless, stringent pollutant reduction requirements combined with new CO_2 mandates draws a challenging scenario, requiring intensive research and development activities to develop and optimize combustion modes to fulfill these requirements. Among the recent advancements, the active pre-chamber ignition system has been considered as a potential alternative to achieve a highly efficient and clean combustion process. Its combustion development is dictated by the pre-chamber ignition system which will provides a high energy flow jet inside the main chamber to enable a multi-site oxidation of the global lean mixture. The comprehension and quantification of the flow and combustion characteristics of the pre-chamber are of utmost importance to optimize the engine operation and pre-chamber design. Nonetheless, restrictive space for instrumentation at experimental side requires alternative numerical methods to aid the quantification of the state parameters and combustion process of these systems. In this sense, this research proposes a novel methodology combining in-cylinder pressure measurement and 1-D simulations as a tool to determine the state, flow and combustion development of different active pre-chambers operating with natural gas in a heavy-duty engine for power generation. The methodology is developed considering 3 different pre-chamber geometries, operating

at different spark timings and equivalence ratios. The results suggest that the methodology is able to quantify the state conditions prior to the spark discharge as well as the evolution of the combustion process by means of considering the perturbations of the mass flow from the pre-chamber inside the main chamber energy balance. Moreover, the methodology allowed to quantify variations of equivalence ratio as small as 0.1 and combustion durations variations of 1 CAD.

1. Introduction

The concern on the rising energy demand associated to the necessity of an expressive reduction of greenhouse gases emission has pushed the investigation efforts towards the utilization of cleaner energy vectors and the optimization of combustion devices [1][2]. In this scenario, natural gas arises as a potential renewable substitute to replace fossil fuels [1]. Natural gas can be obtained from different sources, but biomass-based process enables the most significant benefits on CO_2 reduction [4][5]. Additionally, the conversion of biomass helps to decrease the methane release to the atmosphere, which has a CO_2 potential of 20 [6]. Different studies have demonstrated the practical utilization of natural gas as fuel for spark ignition engines[7][8], attaining benefits in terms of fuel consumption, and given the possibility of knock-free operation at high compression ratio [9][10]. These results suggest that its combination with advanced combustion concepts may lead to even greater benefits [11]. Therefore, the research and development of efficient and cleaner combustion concepts is paramount [12].

In this scenario, different advanced combustion concepts have been recently introduced. Both low temperature [13] and lean combustion [14] concepts are suggested as candidates to achieve efficient combustion while minimizing the production of pollutants as nitrogen oxides (NOx) and soot [15]. The former comprehends several combustion modes, being the homogenous charge compression ignition (HCCI) [16], partially premixed combustion (PPC) [17][18], reactivity compression ignition (RCCI) [19][20][21] and Dual-Mode Dual-Fuel combustion (DMDF) [22][23] some of widely addressed concepts in the literature. On the other hand, lean combustion can be accomplished by different strategies, relying on the equivalence ratio stratification to guarantee a stable flame development from the richer to the leaner zones[24]. Fuel direct injection can be used to create a mixture stratification inside the cylinder that may be used to control the flame development [25]. For lean combustion, the higher oxygen and exhaust gas recirculation dilution (EGR) increases the specific heat ratio, leading to higher efficiencies. Nonetheless, the dilution limits are restricted by combustion variability and flame quenching, leading to unstable and inefficient combustion.

The use of pre-chamber systems has appeared as an alternative to extend the operational limits of lean combustion [26]. This is accomplished due to the multi-site flame development originated by the hot gases torch that leaves the pre-chamber, providing high energy to sustain the oxidation in the main chamber and also a fast combustion compared to conventional spark ignited (SI) engines which decreases the total heat losses [27]. Both passive and active pre-chamber architectures were developed along the years. The former relies on the flow movement inside of the cylinder for the mixture charge and discharge and do not present direct fuel injection on the pre-chamber cavity. This concept allows to extend the equivalence ratio limits but is

highly affected by the scavenging of the pre-chamber, which may produce unstable operation and quenching as the equivalence ratio is decreased. In addition, the equivalence ratios of pre and main chamber are closely related, which contributes to restrict the lean operation limit [28]. By contrast, active pre-chambers employ direct injection of fuel inside the cavity, allowing better control on the local equivalence ratio and decoupling, to a certain degree, the mixture preparation process from the pre and main chambers. In this sense, the pre-chamber can operate at stoichiometric or rich mixtures while maintaining globally lean mixtures in the main chamber. This allows to extend the operation limits, achieving higher efficiencies and lower NOx emissions compared to the passive pre-chamber systems [29].

The pre-chamber combustion, independently on the architecture, is dominated by different parameters such as the turbulence intensity, equivalence ratio, pressure and temperature as well as the residual gas fraction. These parameters will have strong influence on the cycle-to-cycle variability as well as the penetration of the hot gas jet inside the main chamber [30]. Nonetheless, the determination of these properties values is not straightforward. The reduced space for instrumentation generally requires the use of simplified geometries for optical visualization [31][32] or 3-D CFD techniques to quantify the mass transfer between chambers and the state and mixture properties in the pre-chamber. The last provides spatial resolution for the variables of interest but infers high computational time and slows the development process. Therefore, fast analysis and design techniques are needed for early development stages, which may be used to reduce the operating test matrix, to select potential candidates to be investigated in detail and to identify the operating conditions inside the pre-chamber system.

Zero-dimensional combustion modelling coupled to 1-D flow calculations have been extensively used for simplified description of the combustion development in internal combustion engines. The single dependence with respect to time speeds up the solution process at the cost of losing spatial discretization for the solved variables. Despite this, it can provide bulk values of the state parameters and flow characteristics which can be used as guidelines in the design phase. Generally, flow characteristics are calculated by means of finite volume methods, delivering a precise quantification of the intake air flow, residual gases, and equivalence ratio. On the other hand, experimental pressure traces are used to obtain the heat release rates which are imposed in the model to calculate the temperature and heat transfer properties [33]. Since direct instrumentation is a hurdle in pre-chamber system, the combustion description may require its reconstruction by means of derivate quantities.

Despite of not being a predictive technique, combustion description by means of exponential burning laws (Wiebe functions) may be an alternative to reconstruct the pre-chamber combustion development and obtain its state and composition evolution. However, the reconstruction must be derived from the main chamber pressure traces, requiring devising a new methodology which is able to correlate the experimental main chamber results with those of the pre-chamber simulation. In this sense, this research has as aim the development of a methodology to assess the combustion and flow characteristics of a heavy-duty natural gas engine containing an active pre-chamber system. To do this, a 0-D methodology is proposed based on GT-Power modelling of the pre-chamber combustion process by Wiebe functions which are optimized online

applying an external routine developed in Python that consider the perturbations of the mass flow from the pre-chamber inside the main chamber energy balance as a reference for the combustion process definition. The methodology was developed considering three different pre-chamber configurations at a wide range of spark timings and equivalence ratios, guaranteeing the validity of the proposed methodology.

2. Experimental setup

This section details both the experimental and numerical tools and the methodologies that were used during the investigation. First, the engine and experimental facilities are presented. Later, the pre-chamber fuel injection system and the testing methodology is described. Finally, the numerical routines are detailed to evidence the assumptions, limitations, and advantages of the proposed methodology.

2.1. Engine characteristics and test cell description

This investigation was carried out in a single-cylinder engine (SCE) configuration from a commercial Scania D13 6-cylinder heavy-duty compression ignition engine. The main characteristics of the engine are depicted in Table 1. The engine platform modification includes the manufacturing of external air management systems as well as the compression ratio reduction to 12:1 by means of a new set of pistons.

Table 1. Engine characteristics.

Displaced volume [cc]	2124
Stroke [mm]	160
Bore [mm]	130
Connecting Rod [mm]	255
Compression ratio [-]	12:1
Number of Valves	4
Exhaust Valve Open	16.4 CAD bBDC
Intake Valve Close	31 CAD aBDC
Engine speed [rpm]	1500

In addition to this, a pre-chamber system was included into the original cylinder-head. To do so, the diesel injector was removed, and the pre-chamber unit was installed in its respective location by a rework of the original injector housing. The pre-chamber unit includes a 14 mm iridium spark plug placed in an approximately central location, a set of six orifices connecting the pre-chamber with the rest of the cylinder, and a duct for gaseous fuel injection inside the pre-chamber. Three pre-chamber configurations with different orifice diameters, maintaining the rest of the geometry equal. The main specifications of the three pre-chambers are depicted in Table 2.

Table 3. Pre-chamber characteristics.

Parameter	Nozzle 1	Nozzle 2	Nozzle 3
Volume [cm^3]	5.04	5.04	5.04
Number of orifices	6	6	6
Orifice diameter [mm]	1.6	1.8	2.0
Total nozzle cross-section area An [cm^2]	0.0202	0.0254	0.03134
An/Vpc [cm-1]	0.00399	0.00505	0.00623
Vpc/Vc [%]	2.44	2.44	2.44
Material	Nimonic® 80A UNS N07080/W. Nr. 2.4952	Nimonic® 80A UNS N07080/W. Nr. 2.4952	Nimonic® 80A UNS N07080/W. Nr. 2.4952
Thermal conductivity at 20°C [W/mK]	~25	~25	~25

The engine was installed in the test cell facility depicted in Figure 2. The test cell is composed of an external air management system that comprehends a dedicated compressor that allows achieving intake pressures up to 11 bar, a flow meter, an air heating system controlled by a PID (±0.5 °C), two settling chambers and a back-pressure valve to control the exhaust pressure. Moreover, different measurement devices and instrumentation were used. The in-cylinder pressure was measured by means of a Kistler 6053CC transducer. The resultant signals were then correlated to crank angle degrees with a resolution of 0.2 CAD. An AVL i60 emission measurement system was used to quantify the engine-out gaseous emissions as well as the overall equivalence ratio (computed from the oxygen concentration). Finally, different average pressure and temperature sensors were distributed along the intake and exhaust lines to monitor the values of these state variables. Table 3 summarizes some of the relevant instrumentation that was used in this investigation and their respective accuracy.

Table 3. Instrumentation with the respective measurement principle and accuracy.

Variable measured	Device	Manufacturer / model	Accuracy
In-cylinder pressure	Piezoelectric transducer	Kistler / 6053CC	±1.25 %
Intake/exhaust pressure	Piezoresistive transducers	Kistler / 4045A	±25 mbar
Temperature in settling chambers and manifolds	Thermocouple	TC direct / type K	±2.5 °C
Crank angle, engine speed	Encoder	AVL / 364	±0.02 CAD
NOx, CO, HC, O_2, CO_2	Gas analyzer	AVL i60 emission	4%

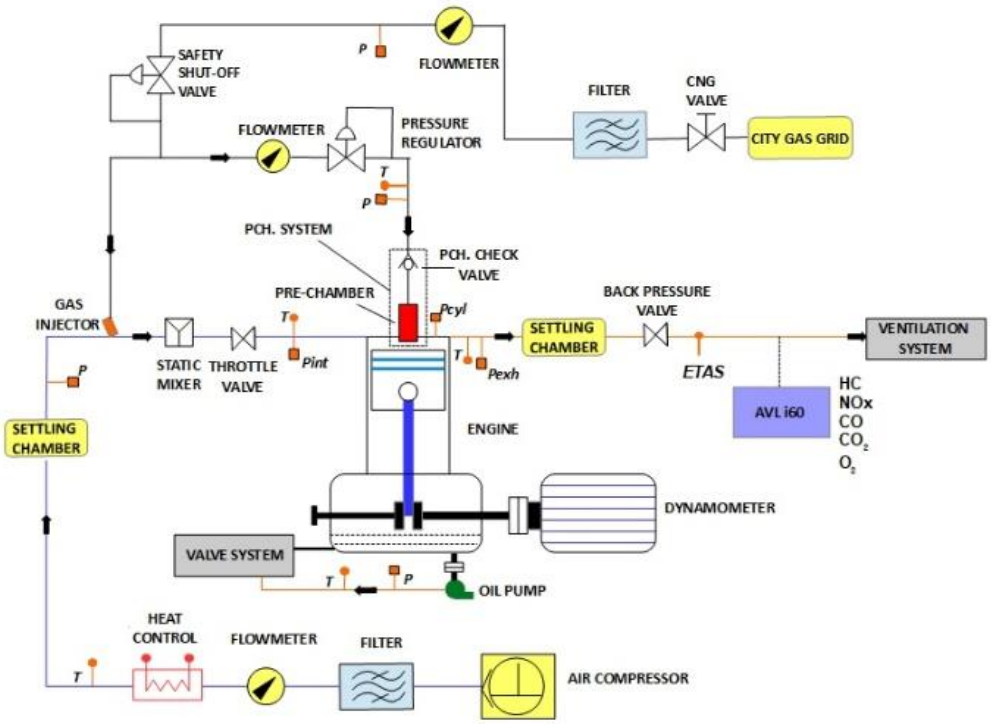

Figure 2. Experimental facility scheme.

Looking at the pre-chamber injection system details in Figure 2, it is possible to observe that the fuel is provided by an external line, from the south-west Swedish national grid. Detailed specifications about the fuel composition and its chemical-physical properties are presented in Onofrio et al. [34]. The same fuel is used to feed both injection systems, the port fuel injection (PFI) and the pre-chamber injection system. The injection process in the pre-chamber is completely defined by means of the pressure difference in the system, as depicted in Figure 3. First, a pressure difference target is defined considering the external delivery system and the injection system. If the pressure difference is higher than 250 mbar, the valve opens and allows the fuel to flow into the injection system. Next, a 558 series check valve by The Lee Company is used to control the fuel flow to the pre-chamber. To do this, a pressure setpoint is specified at 400 mbar. Once the pressure difference between the pre-chamber and the fuel line reaches this setpoint, the fuel injection takes place and is ceased when the pressure difference falls under the target. The fuel flow rate is continuously measured by means of an Emerson Coriolis mass flow meter. In this way, and together with a second flow meter in the overall fuel injection line, it is possible to determine the fuel mass flows going to the pre-chamber and to the rest of the cylinder (though the intake ports), needed for a proper evaluation of the equivalence ratio in both systems.

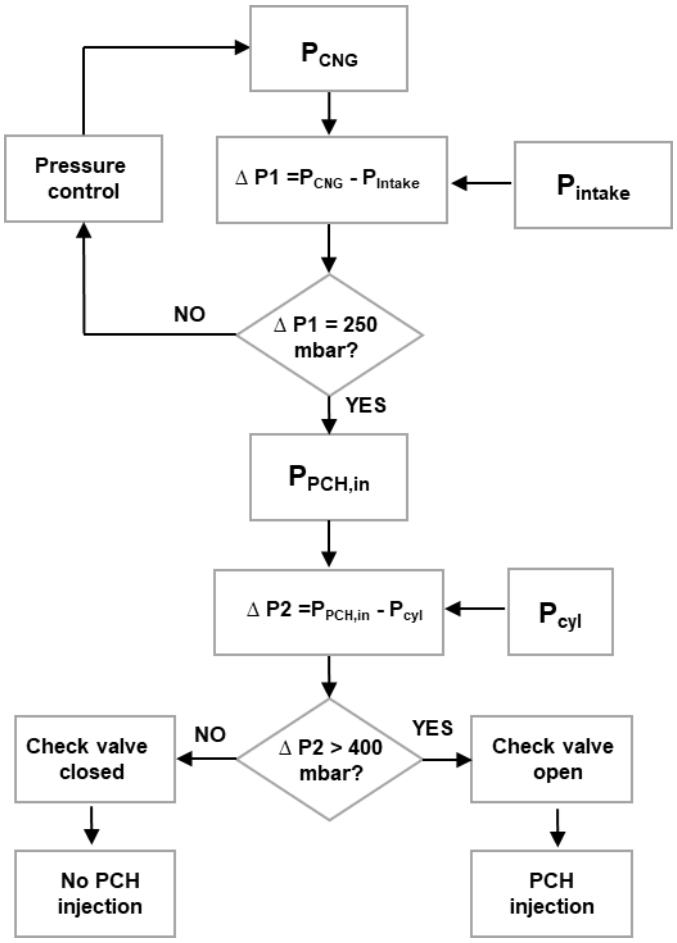

Figure 3. Pre-chamber injection system description.

2.2. Operating condition matrix and testing methodology

The three pre-chambers were evaluated at three different engine loads: 10 bar, 15 bar and 18 bar of indicated mean effective pressure (IMEP). For each engine load, a lambda sweep was performed ranging from 1.5 to 2.1 as always as possible in intervals of 0.2. In addition, a spark sweep was performed for each combination of load and lambda around the optical spark actuation for each engine point and lambda in terms of indicated efficiency.

A specific methodology was developed to ensure stable operating conditions prior to acquire the relevant parameters, as depicted in Figure 4. First, the engine is started at motored condition with an intake pressure of 1.2 bar. Then, both ignition and fuel injection systems are enabled, allowing to run the engine in firing conditions. Once the engine is properly running, both lambda and engine load must be adjusted. While lambda can be obtained by modifying the intake pressure and pre-chamber fuel mass, the engine load generally requires higher amounts of fuel that are provided by the PFI system. Once both lambda and engine load are achieved, the spark timing sweep can be initiated.

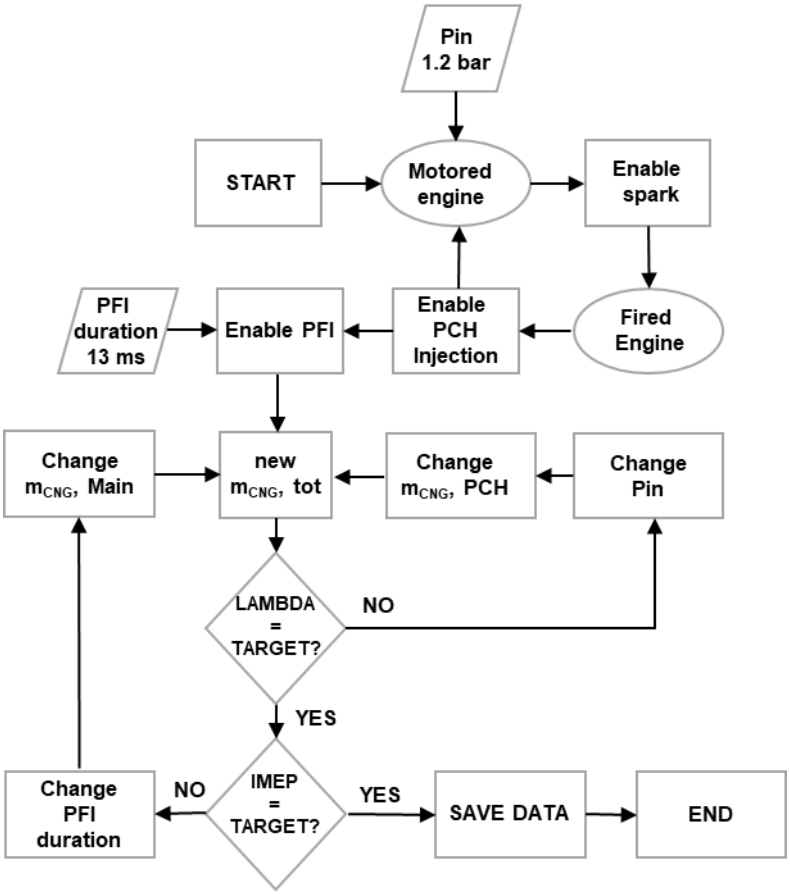

Figure 5. Experimental methodology to assure stable conditions.

2.3. Pre-chamber combustion determination

This section details the methodology developed to assess the global parameters inside the pre-chamber considering the main-chamber instantaneous pressure and the different experimental inputs as boundary conditions. First, the full cycle three pressure analysis routine (TPA) is presented, followed by the discharge time calculation and the adjustment of the pre-chamber combustion parameter by means of an online Python routine coupled to the GT power model.

2.4. Heat release determination and discharge time calculation.

Heat release determination relies on quantifying the energy flows in a closed volume comprehending the combustion system. The most conventional approach to perform this analysis is the application of the first law of thermodynamics subtracting the heat losses, defined as the apparent heat release rate or net heat release rate, which can be easily solved by Equation 1 [35].

$$\frac{dQ_n}{d\theta} = \frac{dQ_{ch}}{d\theta} - \frac{dQ_{ht}}{d\theta} = \frac{\gamma}{\gamma - 1} p \frac{dV}{d\theta} + \frac{1}{\gamma - 1} V \frac{dp}{d\theta} \qquad \text{Equation 1}$$

Where, Q_{ch} is the chemical energy available from the fuel, γ is the ratio of the specific heat at constant pressure and the specific heat at constant volume, p is the in-cylinder pressure, V is the instantaneous volume and θ is the instantaneous crank angle degree.

More detailed approaches quantify the different phenomena that occur during the closed cycle, as heat transfer and fuel evaporation, generally by means of phenomenological correlations. Lastly, full cycle simulations can be used allowing to determine the gas exchange process, detailing the in-cylinder charge composition such as the residuals gas trapped at the cycle start and the fresh-air that is admitted in each cycle. This last approach is fully defined in GT-Power by means of the three-pressure analysis routine, which accounts the intake, exhaust and in-cylinder pressures as boundary conditions for the calculations and was herein used to determine the heat release profiles. A detailed description of the TPA routine can be found in [36]. Figure 6 illustrates the Scania D-13 GT-Power model that was developed to run the TPA calculations.

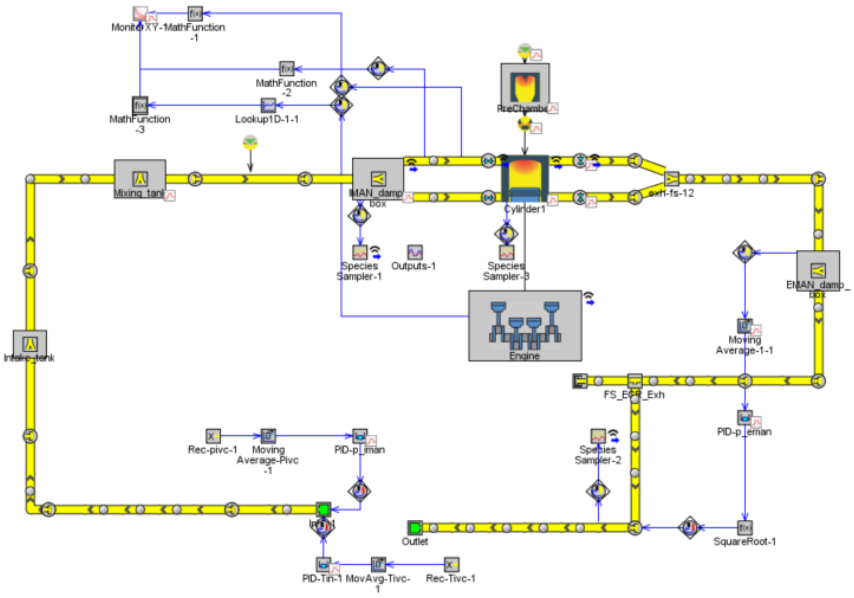

Figure 6. GT-Power model for the Scania D 13 single cylinder engine.

The model consists of specific geometric templates in which the dimensions of each pipe that composes the runners and manifold are specified. In addition, both intake and exhaust lines are modeled. As it can be seen, two PIDs are included in these parts to adjust the average pressure and temperatures at the experimental measurement point. This was implemented because the experimental facility was not able to deliver instantaneous results of manifold pressure. Despite of not being the initial proposal from the TPA, it was previously demonstrated that the solution of the full intake and exhaust path by means of finite volume is able to capture the pressure oscillations from the pulsating flow [37]. A modified Woschni model was used to specify the convective heat transfer coefficient, allowing to calculate the total heat losses during the combustion by means of Equation 2.

$$Q_{HT} = h \cdot A \cdot (T_{cyl} - T_{wall}) \qquad \text{Equation 2}$$

As it can be seen, the total heat transfer is proportional to the wall temperature from the cylinder, piston and cylinder head. Since the measurement of these quantities is not trivial, a detailed finite element model was used considering the coolant temperature

and material properties to obtain spatial resolution of the temperature distributions [38]. This also enables the coupling of the thermal source (cylinder) with the remaining parts as ports and pipes, predicting the wall temperature of each part.

Figure 7 illustrates the comparison of the results obtained from the TPA routine with those from experiments regarding the instantaneous in-cylinder pressure during the full cycle calculation. As it can be observed, the model is able to reproduce with good agreement both the closed cycle and gas exchange. This last presents higher deviations because the instantaneous pressure profiles are not imposed and deviations in the geometry can exist. Moreover, the graph is presented in logarithm scale, which enhances the visualization of small values. However, it should be remarked that the deviations from the experiments in the air flow prediction are lower than 3%, indicating that the gas exchange process model is representative from the experiments. A similar analysis was extended to additional operating conditions, leading to the same conclusions and are not herein presented for brevity sakes.

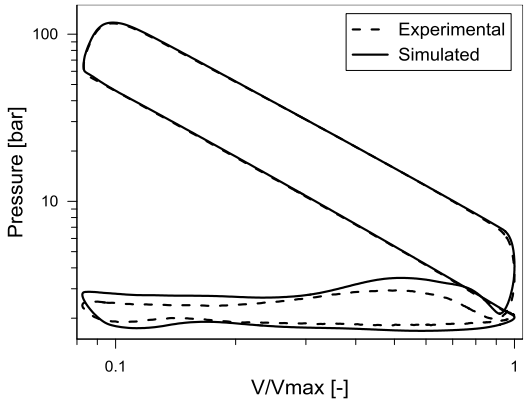

Figure 7. Logarithm of pressure with respect to Logarithm of volume for experimental and simulated conditions.

The application of the TPA routine in each one of the operating conditions allowed to obtain the heat release profiles from the main chamber as depicted in Figure 8. From its analysis, two different slopes can be observed. The first one, with a higher gradient is attributed in the literature to the strong heat delivered once the combustion passes from the pre-chamber to the main chamber, generally called as pre-chamber discharge [39]. Once the discharge finishes and the main chamber combustion progresses, a second small slope period is evidenced in the HRR profiles.

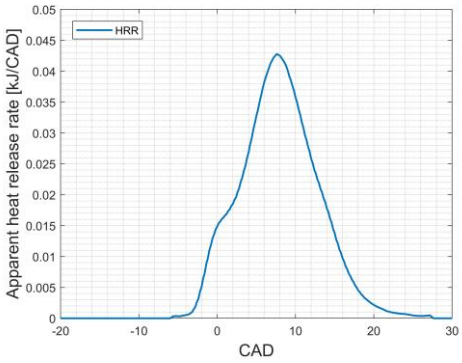

Figure 8. Heat release profiles of the main chamber obtained through the three-pressure analysis simulation.

This two-stage heat release seems to be a direct path to correlate the combustion process from both pre-chamber and main chamber. This link can provide a way to understand the bulk quantities from the pre-chamber by means of an inverse analysis consisting of quantifying the discharge time with the actual combustion duration in the pre-chamber. Relying on the fact that the first derivative of a signal is able to provide the slope changes and its second derivative delivers the crossing zero points, each one of the heat release signals from the different operating conditions was submitted to a MATLAB routine to calculate both derivatives. As depicted in Figure 9 (a), the end of the discharge time is apparent on the first derivative as a local minimum for the first phase of the HRR profile. The crank angle degree determination in which this minimum is located is straightforward. A second derivative can provide the crossing zero points as depicted in Figure 9 (b) and from them, the total duration of the discharge time can be calculated. This routine is extended to the complete dataset, providing the boundary conditions in terms of discharge time to feed the next calculations.

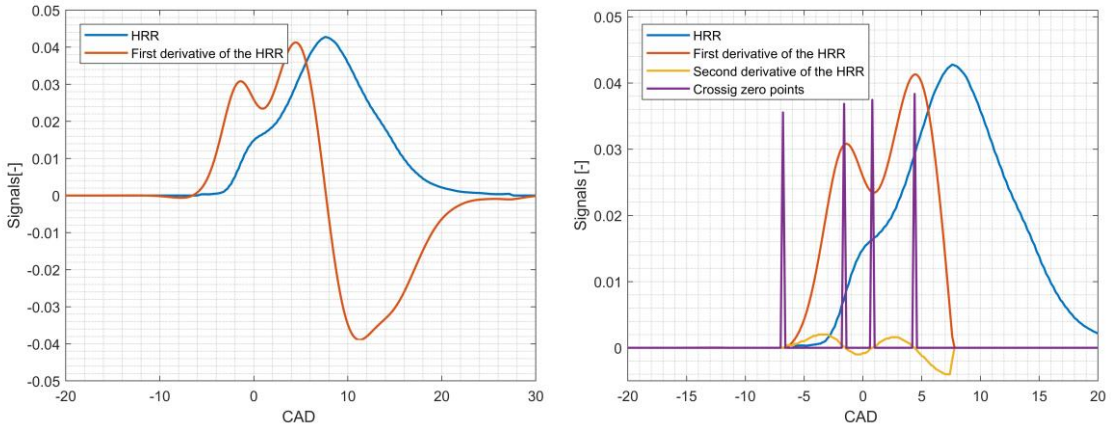

Figure 9. Heat release rate and its first derivate (left); second derivative and crossing zero points (right).

2.5. Pre-chamber combustion adjustment

From a phenomenological point of view, the pre-chamber discharge time duration should be a consequence of the pressure difference from the main chamber and pre-chamber. This is a direct response from the combustion process that initiates in the pre-chamber, increasing the pressure and temperature and creating a gradient between the state properties in both locations during a certain period, which should be similar to the discharge duration. In this sense, it can be argued that if the discharge time is known, it should be possible to reconstruct the combustion process that caused such pressure difference. It should be remarked that a set of assumptions should be made prior to attempting to simulate the pre-chamber combustion.

The combustion in this active pre-chamber initiates from the electrical discharge of the spark plug in a high turbulence environment with a small volume, which provides a fast combustion process. In addition, the small distances from the flame kernel to the walls increases the complexity regarding the flame interactions and the shape of the burning process. Nonetheless, previous results from literature have reported that the combustion still maintains some of the key characteristics of a flame propagation

process [40]. In this sense, the pre-chamber combustion process can be described by a Wiebe function as that presented in Equation 3.

$$x_b = 1 - e^{-a\left(\frac{\theta-\theta_0}{\Delta\theta}\right)^{m+1}} \qquad \text{Equation 3}$$

The use of the Wiebe description requires the knowledge of three different parameters: the combustion duration, and the parameters *a* and *m*. These last are adjustment parameters to fit the slope of the curve. In this research, both parameters are assumed constant and equal to 5 and 2, respectively. This assumption is justified by the data presented in Figure 10, which shows the influence of the factor *m* on the Wiebe shape for two different combustion durations (5 CAD and 15 CAD). As it can be seen, the differences on the combustion development seem to be much less significant for shorter combustion durations (as those presented in the pre-chamber) than for the cases with longer combustion durations. In this sense, it can be concluded that as the combustion duration decreases, lower is the error committed by this assumption. Moreover, the start of the heat release profile should be also defined. In this case, Equation 3 was rearranged to accommodate the CA50 as phasing parameter, allowing to assess the ignition delay values depending on the operating condition. To do this, an additional assumption was made and was then tested during the results discussion. The CA50 values were determined considering half the period of the discharge time, i.e., the maximum discharge rate.

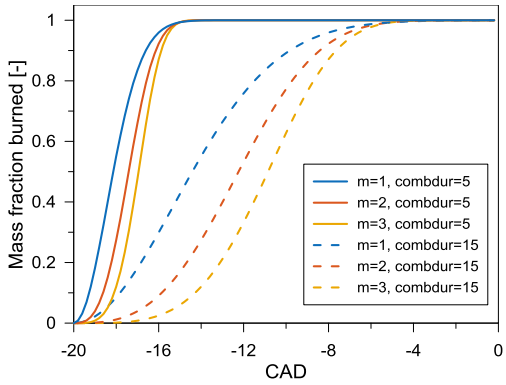

Figure 10. Effect of shape parameter m on the mass fraction burned profiles for two different combustion durations: 5 and 15 CAD.

The only remaining parameter to be adjusted in the equation is the combustion duration. The definition of this parameter was made by means of an iterative routine, coupling a PID controller targeting to achieve the same discharge time than those calculated from the TPA results. To do this, the model from section 2.4 was modified to incorporate a Python routine that allows to include mathematical operations on the mass flow signal, which are not possible by the conventional GT-Power templates. The modified version of the Scania D13 GT Power model is presented in Figure 13.

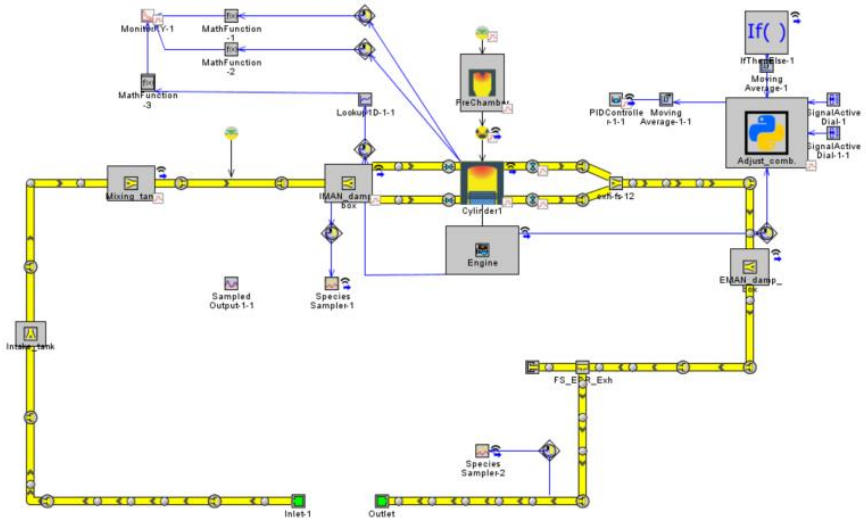

Figure 11. Modified Scania D13 GT-Power model to accounts the online discharge time calculation and pre chamber combustion duration adjustment.

For each cycle, the mass flow through the pre-chamber nozzles was passed to the Python routine allowing to track the instantaneous value of the mass and its derivative. Both indicators were used to identify the flow direction as well as the zero crossing values. In this sense, a logical statement routine was built to find the values in which the signal crosses zero with positive gradient and after the spark timing, indicating the start of the discharge. A similar logical statement was built to determine the end of the discharge time. Figure 12 illustrates the mass flow signal in the pre-chamber nozzle as well as the burn rate profiles from a random iteration.

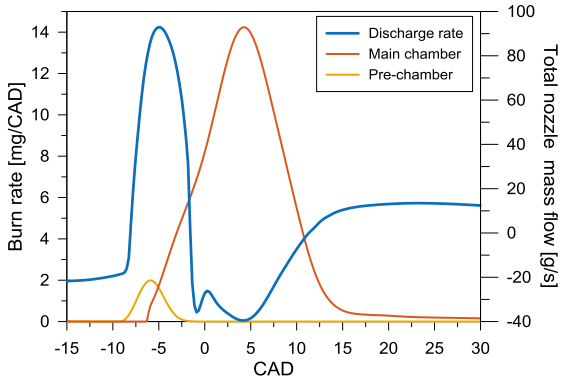

Figure 12. Nozzle mass flow profile, main chamber burn rate and pre-chamber burn rate.

This algorithm was then repeated several times, updating the combustion duration by means of a PID controller which conducts the problem to its solution as depicted in Figure 13. From its analysis, it can be observed that the problem is initiated with a fixed combustion duration. Then, the PID controller starts to have feedback from the Python routine, imposing new values to the combustion duration until the convergence is achieved. The same procedure was then extended to the complete set of operating conditions and nozzle parameters, allowing to investigate the pre-chamber quantities by means of a simplified 1-D calculation routine. It should be remarked that the method does not aims neither to achieve a similar accuracy than that of complex 3-D finite volume domain nor to provide a detailed analysis of local inhomogeneities as both are out of the capability of 1-D modelling.

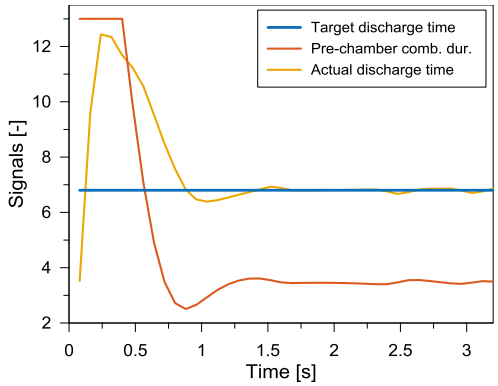

Figure 13. Temporal evolution of the actual discharge time compared to the target as well as the combustion duration evolution.

3. Results

The results section is divided into two different subsections. First, a detailed assessment of the proposed methodology in determining the bulk state and flows parameters for different engine loads is presented for the baseline pre-chamber geometry (PC1). Additionally, the state parameters are used as inputs for the flame speed correlations to assess their relationships with the combustion process that is observed by the methodology application. Finally, the second section intends to compare the effect of using different pre-chamber geometries and the capacity of reconstructing the state parameters by the methodology.

3.1. Baseline geometry (Nozzle 1)

First, the results obtained in terms of the pre-chamber combustion for the first geometry (PC1) will be analyzed. As explained in section 2.2, the test matrix includes 3 levels of engine load (10, 15 and 18 bar IMEP), 4 levels of intake pressure (which imply different overall lambda levels, from 1.5 to 2.1 approximately) and a spark timing sweep for each combination of the aforementioned parameters.

Figure 14 shows the results obtained for the pre-chamber combustion duration in terms of the interval between the 10 and 90% of the heat release rate. In principle, the expectation would be that shorter combustion duration would be induced as the spark is discharged closer to top dead center, as a consequence of the higher in-cylinder temperature, and as the intake pressure is lower, due to richer composition of the charge that travels from the main cylinder to the pre-chamber. This is for instance the trend that can be identified in the case of the 18 bar BMEP condition. However, it has to be considered that there is an interaction between the testing conditions and the equivalence ratio value inside the pre-chamber. On the one hand, delaying the spark implies a longer duration of the filling process from the cylinder to the pre-chamber during the compression stroke. Since the composition inside the cylinder is characterized by a lean mixture, a longer filling process implies a lower equivalence ratio inside the pre-chamber at the spark activation timing. This effect will be more significant as the intake pressure of the test is higher, since it is related with even leaner mixture in the cylinder. On the other hand, as explained in Section 2.1, the pre-chamber fuel injection system is mechanical, so it is affected by the in-cylinder pressure evolution

during the intake process and the beginning of the compression stroke, before the pressure inside the pre-chamber approaches the fuel injection pressure.

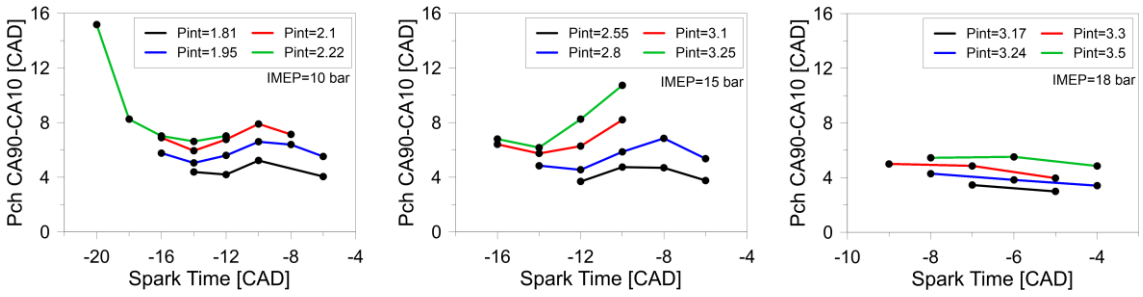

Figure 14. Pre-chamber combustion duration as a function of spark timing. Left: 10 bar IMEP; center: 15 bar IMEP; right: 18 bar IMEP.

Both effects can be seen looking at the equivalence ratio values depicted in Figure 15. First, as anticipated, the equivalence ratio tends to decrease as the spark timing is delayed due to the effect of the longer filling process. Then, higher intake pressure (characterized by leaner conditions inside the cylinder) tends to produce also lower equivalence ratio conditions in the pre-chamber. The range of this variation is reduced as the engine load increases, which is consistent also with the fact that the pre-chamber combustion duration is less sensitive to the variations of the testing conditions at higher load.

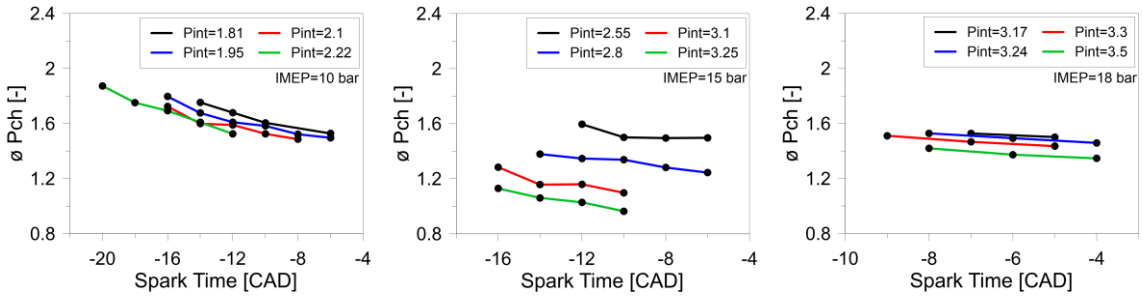

Figure 15. Pre-chamber combustion duration as a function of spark timing. Left: 10 bar IMEP; center: 15 bar IMEP; right: 18 bar IMEP.

One way to better understand the different effects of the equivalence ratio and thermodynamic conditions on the combustion duration inside the pre-chamber is to consider the expected variation in the laminar flame speed. For this purpose, the following correlation previously developed for methane [41] was employed:

$$S_L = S_{L0}\left(\frac{T\ [K]}{298}\right)^{1.7}\left(\frac{p\ [bar]}{1}\right)^{-0.37} \qquad \text{Equation 4}$$

Where *T* and *p* are the pressure and temperature conditions inside the pre-chamber, evaluated in this case at the spark discharge, and S_{L0} represents the laminar flame speed at standard conditions, which is a function of the pre-chamber equivalence ratio according to Equation 5:

$$S_{L0}[m/s] = 0.422\varphi_{Pch}^{-0.15}e^{-5.18(\varphi_{Pch}-1.075)^2} \qquad \text{Equation 5}$$

Figure 16 shows the result of the application of the correlation compared to the pre-chamber combustion duration, confirming that there is a correlation in general between both parameters. Nonetheless, for similar laminar flame speed values there is a clear trend reducing the combustion duration as the load increases, related to the interaction with turbulence generation inside the pre-chamber.

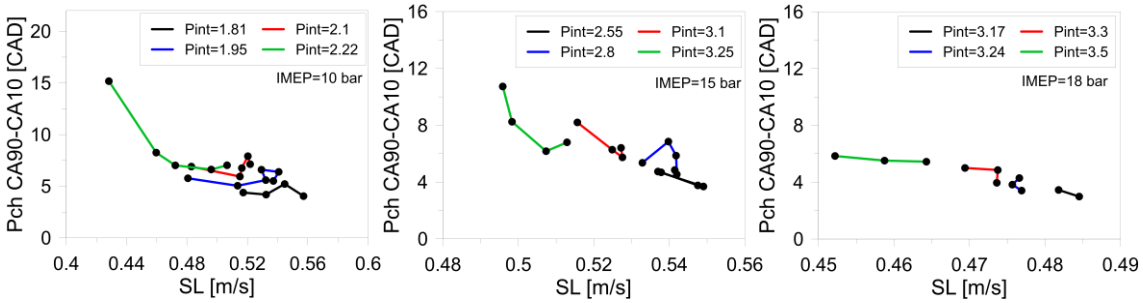

Figure 16. Pre-chamber combustion duration as a function of spark timing. Left: 10 bar IMEP; center: 15 bar IMEP; right: 18 bar IMEP.

Figure 17 shows the information of the discharge velocity of the jet exiting the pre-chamber and the main chamber combustion duration, as a function of the spark timing. As it can be seen, the velocity achieved in this discharge process, which is directly affected by the combustion inside the pre-chamber, drives the main combustion performance. In particular, lower velocity implies lower turbulence generation in the cylinder, enlarging the combustion duration. If these data are compared to the pre-chamber combustion duration depicted in Figure 14, it is visible that higher intake pressure and lower engine load imply a deterioration of both pre- and main chamber combustion timings. This is partially linked to the fact that pre-chamber equivalence ratio is always working in rich conditions, which is not optimal for the pre-chamber combustion process. Therefore, a better equivalence ratio control that could be reached changing the mechanical fuel injection system, currently present with an electronic fuel injection, would help to enhance the pre-chamber combustion system performance. Additionally, higher intake pressure linked to leaner conditions in the main chamber are related to longer main chamber combustion durations, as it could be expected due to the deterioration on flame propagation speed.

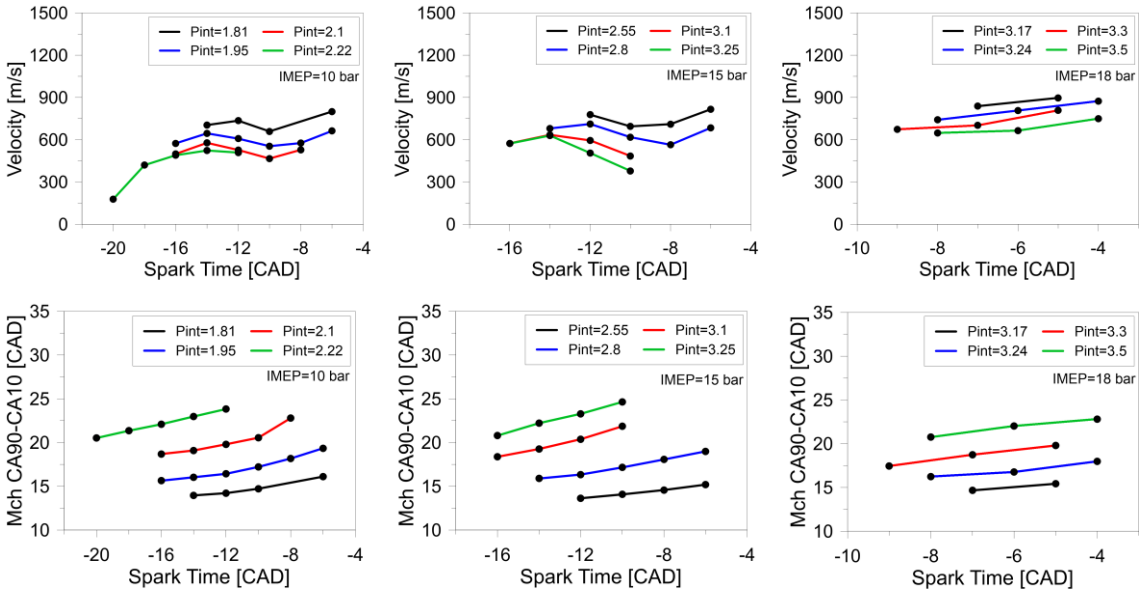

Figure 17. Discharge velocity and main chamber combustion duration as a function of spark timing. Left: 10 bar IMEP; center: 15 bar IMEP; right: 18 bar IMEP.

Finally, Figure 18 shows the engine-out unburned HC and NOx emissions. In general, lean conditions in the main chamber provide lower NOx and higher HC values, according to the expectation. As it can be seen, the two highest intake pressure conditions (which implies an overall equivalence ratio around 0.55 or leaner) are capable to provide almost zero NOx emissions, while maintaining stable combustion. In exchange, a slight deterioration in HC is also detected. However, this deterioration is maintained to a reasonable level as long as the maximum intake pressure (linked to equivalence ratio 0.5) is not reached.

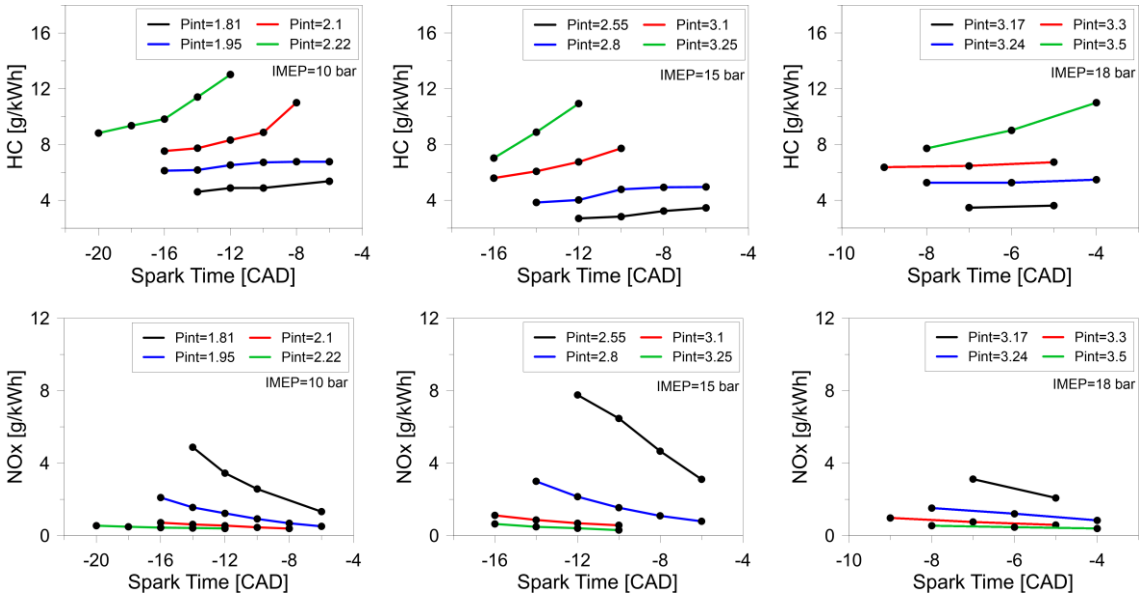

Figure 18. Unburned hydrocarbons and nitrogen oxides emissions as a function of spark timing. Left: 10 bar IMEP; center: 15 bar IMEP; right: 18 bar IMEP.

3.2. Geometry comparison

Once the pre-chamber combustion has been analyzed in detail for the baseline pre-chamber geometry (nozzle 1), this subsection focuses on the effect of the nozzle diameter effect by means of the comparison of the results for the three pre-chamber geometries highlighted in Table 2. Figure 19 shows the evolution of pre-chamber combustion duration and discharge velocity for all three geometries, using the closest possible intake pressure value achieved during the experimental work when trying to maintain the same overall equivalence ratio. In general, it can be seen how the lower orifices diameter is linked to shorter pre-chamber combustion durations, except for the highest load, for which no clear impact is observed. The main reason for this behavior is the turbulence generation inside the pre-chamber. At the same pressure ratio between pre-chamber and the rest of the cylinder, smaller cross-sectional area would imply lower mass flow from the main chamber to the pre-chamber during the compression stroke. Consequently, the pressure evolution in both chambers is more similar one to another, reducing the flow velocity during the pre-chamber filling process. Additionally, lower diameter would be translated into lower size of the vortices produced inside the pre-chamber, reducing turbulence dissipation. Additionally, it can be observed how shorter

pre-chamber combustion duration in terms of CA10-90 is directly linked to higher discharge velocity, as already seen for Nozzle 1.

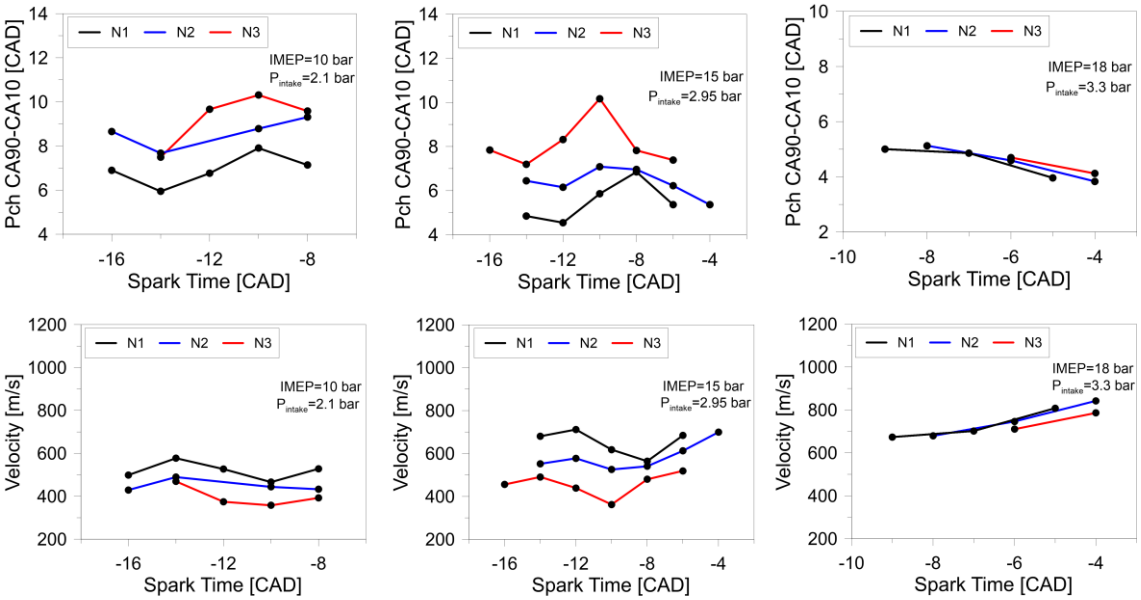

Figure 19. Pre-chamber combustion duration and discharge velocity comparison between pre-chamber geometries. Left: 10 bar IMEP; center: 15 bar IMEP; right: 18 bar IMEP.

The last result of the geometry comparison, focused on the engine-out emissions, is depicted in Figure 20. The results confirmed the aforementioned capability of the current combustion system to significantly reduce the engine-out NOx. However, this effect shows an opposite trend with respect to the pre-chamber combustion duration and velocity previously discussed. Highest discharge velocity would result in increased turbulence inside the main chamber, maximizing turbulence and shortening the main combustion duration. This is consistent with the reduction in the unburned HC emissions, as a consequence of the positive impact of higher combustion velocity on the quenching distance. But shortening the main combustion implies also an increase of the maximum in-cylinder temperature, which directly drives the NOx emissions through Zeldovich's mechanism. Consequently, the pre-chamber cross-sectional area shall be selected considering the trade-off between the combustion duration and NOx emissions, especially if such combustion strategy is selected as a mean to achieve engine certification together without specific NOx aftertreatment system, which is critical for lean combustion operation.

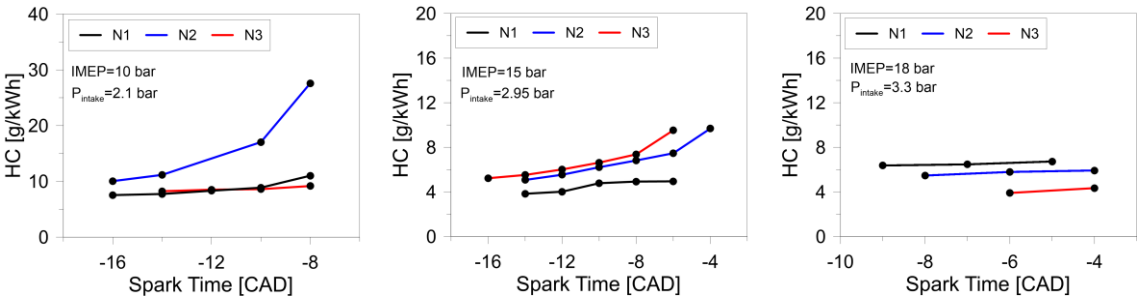

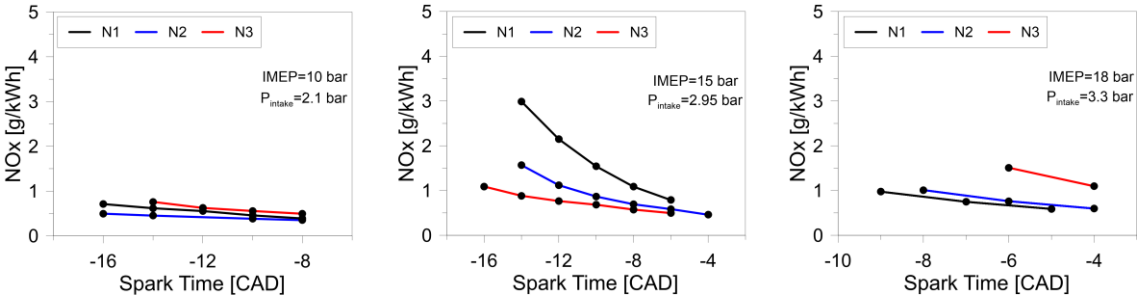

Figure 20. Unburned hydrocarbons and nitrogen oxides comparison between pre-chamber geometries. Left: 10 bar IMEP; center: 15 bar IMEP; right: 18 bar IMEP.

4. Conclusions

This work has proposed a novel methodology aiming at the determination of the flow and state parameters inside the pre-chamber and a reconstruction of the combustion process by coupling GT-Power model and Python scripting. The methodology has been validated and applied for conditions addressing different engine loads and pre-chamber nozzles. Moreover, the several equivalence ratios and spark timings were included in the assessment. The application of the methodology has allowed to draw important conclusions:

- The methodology is useful to quantify important flow and state characteristics inside the pre-chamber prior to the spark discharge. These parameters dictate the pre-chamber combustion development, demonstrating a strong correlation with the adjusted pre-chamber combustion duration.
- The impact of operating parameters, such as intake pressure, engine load and spark timing were captured by the proposed methodology.
- The modification of the geometric characteristics such as the nozzle diameter was modelled by the methodology, enabling the reconstruction of the combustion process.

The results have also evidenced that the use of the methodology has enabled the quantification of the equivalence ratio in the pre-chamber and its respective combustion process. Moreover, it was demonstrated the interplay of nozzle velocity and equivalence ratio in the pre-chamber with the results found in the main chamber combustion and consequent emission formation. In this sense, it can be concluded that the proposed framework is a useful tool to aid the investigation of pre-chamber ignition system aiming at identifying parameters that are difficult to measure experimentally. This helps to quantify bulk conditions which are important to extend the operating limits towards lean operation to achieve a cleaner and efficient combustion.

5. Bibliography

[1] R. Payri, J. De La Morena, J. Monsalve-Serrano, F.C. Pesce, A. Vassallo, Impact of counter-bore nozzle on the combustion process and exhaust emissions for light-duty diesel engine application, Int. J. Engine Res. 20 (2019) 46–57. doi:10.1177/1468087418819250.

[2] V. Bermúdez, A. García, D. Villalta, L. Soto, Assessment on the consequences of injection strategies on combustion process and particle size distributions in Euro VI medium-duty diesel engine, Int. J. Engine Res. 21 (2020) 683–697. doi:10.1177/1468087419865652.

[3] A. Rimkus, S. Stravinskas, J. Matijošius, Comparative study on the energetic and ecologic parameters of dual fuels (diesel-NG and HVO-biogas) and conventional diesel fuel in a CI engine, Appl. Sci. 10 (2020). doi:10.3390/app10010359.

[4] S. Xue, J. Song, X. Wang, Z. Shang, C. Sheng, C. Li, Y. Zhu, J. Liu, A systematic comparison of biogas development and related policies between China and Europe and corresponding insights, Renew. Sustain. Energy Rev. 117 (2020) 109474. doi:10.1016/j.rser.2019.109474.

[5] S. Achinas, V. Achinas, G.J.W. Euverink, A Technological Overview of Biogas Production from Biowaste, Engineering. 3 (2017) 299–307. doi:10.1016/J.ENG.2017.03.002.

[6] O. Boucher, P. Friedlingstein, B. Collins, K.P. Shine, The indirect global warming potential and global temperature change potential due to methane oxidation, Environ. Res. Lett. 4 (2009). doi:10.1088/1748-9326/4/4/044007.

[7] R.B.R. da Costa, J.J. Hernández, A.F. Teixeira, N.A.D. Netto, R.M. Valle, V.R. Roso, C.J.R. Coronado, Combustion, performance and emission analysis of a natural gas-hydrous ethanol dual-fuel spark ignition engine with internal exhaust gas recirculation, Energy Convers. Manag. 195 (2019) 1187–1198. doi:10.1016/j.enconman.2019.05.094.

[8] S. Szwaja, E. Ansari, S. Rao, M. Szwaja, K. Grab-Rogalinski, J.D. Naber, M. Pyrc, Influence of exhaust residuals on combustion phases, exhaust toxic emission and fuel consumption from a natural gas fueled spark-ignition engine, Energy Convers. Manag. 165 (2018) 440–446. doi:10.1016/j.enconman.2018.03.075.

[9] X. Kan, D. Zhou, W. Yang, X. Zhai, C.H. Wang, An investigation on utilization of biogas and syngas produced from biomass waste in premixed spark ignition engine, Appl. Energy. 212 (2018) 210–222. doi:10.1016/j.apenergy.2017.12.037.

[10] E. Porpatham, A. Ramesh, B. Nagalingam, Effect of hydrogen addition on the performance of a biogas fuelled spark ignition engine, Int. J. Hydrogen Energy. 32 (2007) 2057–2065. doi:10.1016/j.ijhydene.2006.09.001.

[11] I.D. Bedoya, S. Saxena, F.J. Cadavid, R.W. Dibble, M. Wissink, Experimental study of biogas combustion in an HCCI engine for power generation with high indicated efficiency and ultra-low NOx emissions, Energy Convers. Manag. 53 (2012) 154–162. doi:10.1016/j.enconman.2011.08.016.

[12] Belgiorno G, Dimitrakopoulos N, Di Blasio G, Beatrice C, Tunestål P, Tunér M. Effect of the engine calibration parameters on gasoline partially premixed combustion performance and emissions compared to conventional diesel combustion in a light-duty Euro 6 engine. Appl Energy 2018;228:2221–34. https://doi.org/10.1016/j.apenergy.2018.07.098

[13] M. Krishnamoorthi, R. Malayalamurthi, Z. He, S. Kandasamy, A review on low temperature combustion engines: Performance, combustion and emission characteristics, Renew. Sustain. Energy Rev. 116 (2019) 109404. doi:10.1016/j.rser.2019.109404.

[14] F. Leach, G. Kalghatgi, R. Stone, P. Miles, The scope for improving the efficiency and environmental impact of internal combustion engines, Transp. Eng. 1 (2020) 100005. doi:10.1016/j.treng.2020.100005.

[15] J. Benajes, A. García, J. Monsalve-Serrano, R. Sari, Clean and efficient dual-fuel combustion using OMEx as high reactivity fuel: Comparison to diesel-gasoline calibration, Energy Convers. Manag. 216 (2020) 112953. doi:10.1016/j.enconman.2020.112953.

[16] M. Martins, I. Fischer, F. Gusberti, R. Sari, M.D. Nora, HCCI of Wet Ethanol on a Dedicated Cylinder of a Diesel Engine, SAE Tech. Pap. 2017-March (2017). doi:10.4271/2017-01-0733.

[17] S. Molina, A. García, J. Monsalve-Serrano, D. Villalta, Effects of fuel injection parameters on premixed charge compression ignition combustion and emission characteristics in a medium-duty compression ignition diesel engine, Int. J. Engine Res. 22 (2021) 443–455. doi:10.1177/1468087419867014.

[18] Monsalve-Serrano J, Belgiorno G, Di Blasio G, Guzmán-Mendoza M. 1D simulation and experimental analysis on the effects of the injection parameters in methane–diesel dual-fuel combustion. Energies 2020;13:1–13. https://doi.org/10.3390/en13143734.

[19] R.D. Reitz, G. Duraisamy, Review of high efficiency and clean reactivity controlled compression ignition (RCCI) combustion in internal combustion engines, Prog. Energy Combust. Sci. 46 (2015) 12–71. doi:10.1016/j.pecs.2014.05.003.

[20] J. Benajes, A. García, J. Monsalve-Serrano, R. Sari, Potential of RCCI Series Hybrid Vehicle Architecture to Meet the Future CO2 Targets with Low Engine-Out Emissions, Appl. Sci. 8 (2018) 1472. doi:10.3390/app8091472.

[21] J. Benajes, A. García, J. Monsalve-Serrano, R. Lago Sari, Fuel consumption and engine-out emissions estimations of a light-duty engine running in dual-mode RCCI/CDC with different fuels and driving cycles, Energy. 157 (2018) 19–30. doi:10.1016/j.energy.2018.05.144.

[22] A. García, J. Monsalve-Serrano, S. Martinez-Boggio, P. Gaillard, O. Poussin, A.A. Amer, Dual fuel combustion and hybrid electric powertrains as potential solution to achieve 2025 emissions targets in medium duty trucks sector, Energy Convers. Manag. 224 (2020) 113320. doi:10.1016/j.enconman.2020.113320.

[23] A. García, J. Monsalve-Serrano, D. Villalta, R. Sari, Fuel sensitivity effects on dual-mode dual-fuel combustion operation for different octane numbers, Energy Convers. Manag. 201 (2019). doi:10.1016/j.enconman.2019.112137.

[24] G. Marseglia, M. Costa, F. Catapano, P. Sementa, B.M. Vaglieco, Study about the link between injection strategy and knock onset in an optically accessible multi-cylinder GDI engine, Energy Convers. Manag. 134 (2017) 1–19. doi:10.1016/j.enconman.2016.12.012.

[25] T. Nagasawa, Y. Okura, R. Yamada, S. Sato, H. Kosaka, T. Yokomori, N. Iida, Thermal efficiency improvement of super-lean burn spark ignition engine by stratified water insulation on piston top surface, Int. J. Engine Res. (2020) 2–12. doi:10.1177/1468087420908164.

[26] E. Distaso, R. Amirante, E. Cassone, P. De Palma, P. Sementa, P. Tamburrano, B.M. Vaglieco, Analysis of the combustion process in a lean-burning turbulent jet ignition engine fueled with methane, Energy Convers. Manag. 223 (2020) 113257. doi:10.1016/j.enconman.2020.113257.

[27] R. Novella, J. Gomez-Soriano, P.J. Martinez-Hernandiz, C. Libert, F. Rampanarivo, Improving the performance of the passive pre-chamber ignition concept for spark-ignition engines fueled with natural gas, Fuel. 290 (2021) 119971. doi:10.1016/j.fuel.2020.119971.

[28] J. Benajes, R. Novella, J. Gomez-Soriano, I. Barbery, C. Libert, F. Rampanarivo, M. Dabiri, Computational assessment towards understanding the energy conversion and combustion process of lean mixtures in passive pre-chamber ignited engines, Appl. Therm. Eng. 178 (2020) 115501. doi:10.1016/j.applthermaleng.2020.115501.

[29] C. Müller, S. Pischinger, S. Tews, A. Müller, K. Habermann, Analysis of experimental results with an active pre-chamber ultra-lean burn SI engine, Int. J. Engine Res. (2020). doi:10.1177/1468087420974544.

[30] J.M. Desantes, J.J. López, R. Novella, J. Antolini, Pre-chamber ignition systems: A methodological proposal to reproduce a reference case in a simplified experimental facility for fundamental studies, Int. J. Engine Res. (2020). doi:10.1177/1468087420971115.

[31] J.M. Desantes, R. Novella, J. De La Morena, V. Pagano Lng, Achieving ultra-lean combustion using a pre-chamber spark ignition system in a rapid compression-expansion machine, SAE Tech. Pap. 2019-April (2019) 1–12. doi:10.4271/2019-01-0236.

[32] M. Echeverri Marquez, P. Hlaing, Q. Tang, R. Sampath, E. Cenker, M. Ben Houidi, G. Magnotti, B. Johansson, High-Speed Imaging of Main-Chamber Combustion of a Narrow Throat Pre-Chamber under Lean Conditions, SAE Tech. Pap. (2020) 1–13. doi:10.4271/2020-01-2081.

[33] Z. Şahin, O. Durgun, O.N. Aksu, Experimental investigation of n-butanol/diesel fuel blends and n-butanol fumigation - Evaluation of engine performance, exhaust emissions, heat release and flammability analysis, Energy Convers. Manag. 103 (2015) 778–789. doi:10.1016/j.enconman.2015.06.089.

[34] G. Onofrio, C. Li, P. Garcia Valladolid, J. De La Morena, A. Garcia, P. Tunestal, C. Beatrice, Experimental and Numerical Assessment of Active Pre-chamber Ignition in Heavy Duty Natural Gas Stationary Engine, SAE Tech. Pap. 2020-April (2020) 1–14. doi:10.4271/2020-01-0819.

[35] J.B. Heywood, Internal Combustion Engine Fundamentals, McGraw Hill, 1988.

[36] Gamma Technologies, Engine Performance Application Manual, (2016).

[37] T.D.M. Lanzanova, M. Dalla Nora, M.E.S. Martins, P.R.M. Machado, V.B. Pedrozo, H. Zhao, The effects of residual gas trapping on part load performance and emissions of a spark ignition direct injection engine fuelled with wet ethanol, Appl. Energy. 253 (2019) 113508. doi:10.1016/j.apenergy.2019.113508.

[38] R.K. T. Morel, C.I.Rackmil, M.J. Jennings, Model for Heat Transfer and Combustion in Spark Ignited Engines and Its Comparison with Experiments, SAE Tech. Pap. Ser. (1988).

[39] C.E.C. Alvarez, G.E. Couto, V.R. Roso, A.B. Thiriet, R.M. Valle, A review of prechamber ignition systems as lean combustion technology for SI engines, Appl. Therm. Eng. 128 (2018) 107–120. doi:10.1016/j.applthermaleng.2017.08.118.

[40] Q. Malé, G. Staffelbach, O. Vermorel, A. Misdariis, F. Ravet, T. Poinsot, Large Eddy Simulation of Pre-Chamber Ignition in an Internal Combustion Engine, Flow, Turbul. Combust. 103 (2019) 465–483. doi:10.1007/s10494-019-00026-y.

[41] R. Amirante, E. Distaso, P. Tamburrano, R.D. Reitz, Laminar flame speed correlations for methane, ethane, propane and their mixtures, and natural gas and gasoline for spark-ignition engine simulations, Int. J. Engine Res. 18 (2017) 951–970. doi:10.1177/1468087417720018.

Abbreviatures

CAD	Crank Angle Degree
CFD	Computational Fluid Dynamics
CO	Carbon Monoxide
CO2	Carbon Dioxide
DMDF	Dual Mode Dual Fuel
EGR	Exhaust Gas Recirculation
HC	Unburned Hydrocarbons
HCCI	Homogeneous charge compression ignition
IMEP	Indicated Mean Effective Pressure
N	Nozzle
NOx	Nitrogen Oxides
PC	Pre-Chamber
PFI	Port Fuel Injection
PID	Proportional Integral Derivative
PPC	Partially Premixed Combustion
SCE	Single Cylinder Engine
SI	Spark Ignition
TPA	Three Pressure Analysis